Research Article | Vol. 9, No. 4 | 1 Apr 2018 | BIOMEDICAL OPTICS EXPRESS 1948
Biomedical Optics EXPRESS

Efficiency of ocular UV protection by clear lenses

KATHARINA RIFAI,[1,2,5,6] MATTHIAS HORNAUER,[3,5,7] RAMONA BUECHINGER,[3] ROLAND SCHOEN,[3] MARIA BARRAZA-BERNAL,[1] SELAM HABTEGIORGIS,[1] CARSTEN GLASENAPP,[4] SIEGFRIED WAHL,[1,2] AND TIMO MAPPES[2]

[1]*Institute for Ophthalmic Research, University of Tuebingen, Tuebingen, Germany*
[2]*Carl Zeiss Vision International GmbH, Aalen, Germany*
[3]*Carl Zeiss Vision GmbH, Aalen, Germany*
[4]*Carl Zeiss AG, Oberkochen, Germany*
[5]*These authors contributed equally*
[6]*katharina.rifai@medizin.uni-tuebingen.de*
[7]*matthias.hornauer@zeiss.com*

Abstract: Ocular UV doses accumulate all-day, not only during periods of direct sun exposure. The UV protection efficiency of three clear lenses was evaluated experimentally, validated by simulation, and compared to non-UV protection: a first spectacle lens with a tailored UV absorber, a second spectacle lens, minimizing UV back reflections, as well as a third spectacle lens, combining both. A tailored UV-absorber efficiently reduced overall UV irradiance to 7 %, whereas reduction of back-reflections still left UV irradiance at 42 %. Thus, clear lenses with a tailored UV absorber efficiently protect the eye from UV, supplementing sun glasses wear to an all-day protection scenario.

OCIS codes: (330.4460) Ophthalmic optics and devices; (330.5370) Physiological optics; (330.7328) Visual optics, ophthalmic appliances; (140.3360) Laser safety and eye protection.

References and links

1. J. C. Yam and A. K. Kwok, "Ultraviolet light and ocular diseases," International Ophthalmology **34**, 383–400 (2014).
2. P. Gies, "Ultraviolet protection factors for clothing: An intercomparison of measurement systems," J. Photochem. Photobiol. **77.1**, 58–67 (2003).
3. P. J. Matts, V. Alard, M. W. Brown, L. Ferrero, H. Gers-Barlag, N. Issachar, D. Moyal, and R. Wolber, "The COLIPA in vitro UVA method: a standard and reproducible measure of sunscreen UVA protection," Int. J. Cosmet. Sci. **32**, 35–46 (2010).
4. G. W. Hall and M. Schultmeyer, "The FUBI system for solar rating nonprescription eyewear," Optometry (St. Louis, Mo.) **73**, 407–417 (2002).
5. S. J. Dain, "Sunglasses and sunglass standards," Clin. Exp. Ophthalmol. **86**, 77–90 (2003).
6. International Commission on Non-Ionizing Radiation Protection, "Guidelines on limits of exposure to ultraviolet radiation of wavelengths between 180 nm and 400 nm (incoherent optical radiation)," Health Physics **87**, 171–186 (2004).
7. N. Pakrou, R. Casson, S. Fung, N. Ferdowsi, G. Lee, and D. Selva, "South Australian adolescent ophthalmic sun protective behaviours," Eye **22**, 808–814 (2008).
8. B. S. B. Wachler, "Assessment of levels of ultraviolet a light protection in automobile windshields and side windows," JAMA Ophthalmol. **134**, 772–775 (2016).
9. F. Almutawa, R. Vandal, S. Q. Wang, and H. W. Lim, "Current status of photoprotection by window glass, automobile glass, window films, and sunglasses," Photodermatol. Photoimmunol. Photomed. **29**, 65–72 (2013).
10. C. Tuchinda, S. Srivannaboon, and H. W. Lim, "Photoprotection by window glass, automobile glass, and sunglasses," J. Am. Acad. Dermatol. **54**, 845–854 (2006).
11. E. Thieden, P. A. Philipsen, J. Heydenreich, and H. C. Wulf, "UV radiation exposure related to age, sex, occupation, and sun behavior based on time-stamped personal dosimeter readings," Arch. Dermatol. **140**, 197–203 (2004).
12. M. G. Kimlin, A. V. Parisi, and J. C. F. Wong, "Quantification of personal solar UV exposure of outdoor workers, indoor workers and adolescents at two locations in southeast Queensland," Photodermatol. Photoimmunol. Photomed. **14**, 7–11 (1998).

#320710 https://doi.org/10.1364/BOE.9.001948
Journal © 2018 Received 26 Jan 2018; revised 14 Mar 2018; accepted 16 Mar 2018; published 27 Mar 2018

Biomedical Optics EXPRESS

13. International Commission on Illumination 1–48, "Colorimetry, CIE Tech. Rep. CIE 15:2004, 3rd ed," Tech. Rep. (2004).
14. F. S. Rosenthal, A. E. Bakalian, and H. R. Taylor, "The effect of prescription eyewear on ocular exposure to ultraviolet radiation," Am. J. Public Health **76**, 1216–1220 (1986).
15. S. Abdulrahim, Y. M. Abubakar, and I. T. Bello, "Evaluation of the level of transmission of solar radiation by eyeglasses (spectacles) and its effects on the human eye," JASR **5**, 489–498 (2015).
16. D. G. Pitts, "Ultraviolet-absorbing spectacle lenses, contact lenses, and intraocular lenses," Optom. Vis. Sci. **67**, 435–440 (1990).
17. J.-C. Liou, M.-C. Teng, Y.-S. Tsai, E.-C. Lin, and B.-Y. Chen, "UV-blocking spectacle lens protects against uv-induced decline of visual performance," Molecular Vision **21**, 846–856 (2015).
18. F. Behar-Cohen, G. Baillet, T. de Ayguavives, P. O. Garcia, J. Krutmann, P. Pena-Garcia, C. Reme, and J. S. Wolffsohn, "Ultraviolet damage to the eye revisited: eye-sun protection factor (e-spf), a new ultraviolet protection label for eyewear," Clin. Ophthalmol. **8**, 87–104 (2014).
19. J. Krutmann, F. Behar-Cohen, G. Baillet, T. de Ayguavives, P. Ortega Garcia, P. Pena-Garcia, C. Reme, and J. Wolffsohn, "Towards standardization of UV eye protection: what can be learned from photodermatology?" Photodermatol. Photoimmunol. Photomed. **30**, 128–136 (2014).
20. D. H. Sliney, "Photoprotection of the eye- UV radiation and sunglasses," J. Photochem. Photobiol. B: Biology **64**, 166–175 (2001).
21. Y. Sakamoto, M. Kojima, and K. Sasaki, "Effectiveness of eyeglasses for protection against ultraviolet rays," Jpn. J. Ophthalmol. **43**, 566–567 (1999).
22. G.-C. Liu, F. Wang, Y.-Y. Gao, Z. Yang, L.-W. Hu, Q. Gao, J.-C. Ri, and Y. Liu, "The enhancement of biological ocular UV radiation on beaches compared to the radiation on grass," J. Photochem. Photobiol. B: Biology **141**, 106–112 (2014).
23. P. Weihs, "Influence of ground reflectivity and topography on erythemal UV radiation on inclined planes," Int. J.Biometeorol. **46**, 95–104 (2002).
24. F. S. Rosenthal, C. Phoon, A. E. Bakalian, and H. R. Taylor, "The ocular dose of ultraviolet radiation to outdoor workers," Invest. Ophthalmol. Vis. Sci.**29**, 649–656 (1988).
25. P. Weihs, A. Schmalwieser, C. Reinisch, E. Meraner, S. Walisch, and M. Harald, "Measurements of personal UV exposure on different parts of the body during various activities," Photochem. Photobiol. **89**, 1004–1007 (2013).
26. E. Herlihy, P. H. Gies, C. R. Roy, and M. Jones, "Personal dosimetry of solar UV radiation for different outdoor activities," Photochem. Photobiol.**60**, 288–294 (1994).
27. K. A. Baczynska, A. J. Pearson, J. B. O'Hagan, and J. Heydenreich, "Effect of altitude on solar UVR and spectral and spatial variations of UV irradiances measured in Wagrain, Austria in winter," Radiation Protection Dosimetry **154**, 497–504 (2012).
28. J. Kim, H.-K. Cho, J. Mok, H. D. Yoo, and N. Cho, "Effects of ozone and aerosol on surface UV radiation variability," J. Photochem. Photobiol. B: Biology **119**, 46–51 (2013).
29. A. Oppenrieder, P. Hoeppe, and P. Koepke, "Routine measurement of erythemally effective UV irradiance on inclined surfaces," J. Photochem. Photobiol. B: Biology **74**, 85–94 (2004).
30. J. Turner, A. V. Parisi, and D. J. Turnbull, "Reflected solar radiation from horizontal, vertical and inclined surfaces: Ultraviolet and visible spectral and broadband behaviour due to solar zenith angle, orientation and surface type," J. Photochem. Photobiol. B: Biology **92**, 29–37 (2008).
31. J. Turner and A. V. Parisi, "Measuring the influence of UV reflection from vertical metal surfaces on humans," Photochem. Photobiol. Sci. **8**, 62–69 (2009).
32. L. Hu, Q. Gao, N. Gao, G. Liu, Y. Wang, H. Gong, and Y. Liu, "Solar UV exposure at eye is different from environmental UV: diurnal monitoring at different rotation angles using a mannequin," J. Occup. Environ. Hyg. **10**, 17–25 (2013).
33. L. Hu, F. Wang, N.-N. Ou-Yang, N. Gao, Q. Gao, T. Ge, Y. Gao, G. Liu, Y. Zheng, and Y. Liu, "Quantification of ocular biologically effective UV exposure for different rotation angle ranges based on data from a mannequin," Photochem. Photobiol. **90**, 925–934 (2014).
34. N. Gao, L.-W. Hu, Q. Gao, T.-T. Ge, F. Wang, C. Chu, H. Yang, and Y. Liu, "Diurnal variation of ocular exposure to solar ultraviolet radiation based on data from a mannequin head," Photochem. Photobiol. **88**, 736–743 (2012).
35. H. Sasaki, Y. Sakamoto, C. Schnider, N. Fujita, N. Hatsusaka, D. H. Sliney, and K. Sasaki, "UV-b exposure to the eye depending on solar altitude," Eye & Contact Lens **37**, 191–195 (2011).
36. L. M. Garrison, L. E. Murray, D. D. Doda, and A. E. S. Green, "Diffuse & direct ultraviolet ratios with a compact double monochromator," Appl. Opt. **17**, 827–836 (1978).
37. P. Koepke and M. Mech, "UV irradiance on arbitrarily oriented surfaces: variation with atmospheric and ground properties," Theor. Appl. Climatol. **81**, 25–32 (2005).
38. D. Vernez, A. Milon, L. Vuilleumier, and J.-L. Bulliard, "Anatomical exposure patterns of skin to sunlight: relative contributions of direct, diffuse and reflected ultraviolet radiation," Br. J. Dermatol. **167**, 383–390 (2012).
39. J. Yu, H. Hua, Y. Liu, and Y. Liu, "Distributions of direct, reflected, and diffuse irradiance for ocular UV exposure at different solar elevation angles," PloS one **11**, e0166729 (2016).
40. S. Usumez, T. Uysal, M. Orhan, and E. Soganci, "Relationship between static natural head position and head position measured during walking," Am. J. Orthod. Dentofac. Orthop **129**, 42–47 (2006).

Biomedical Optics EXPRESS

41. D. P. Fleming, J. E. Walsh, L. A. Moore, J. P. Bergmanson, and D. McMahon, "A novel sensor array for field based ocular ultraviolet radiation measurements," Radiation Protection Dosimetry **118**, 265–274 (2005).
42. J. J. Streicher, W. C. Culverhouse, M. S. Dulberg, and R. J. Fornaro, "Modeling the anatomical distribution of sunlight," Photochem. Photobiol. **79**, 40–47 (2004).
43. P. Hoeppe, A. Oppenrieder, C. Erianto, P. Koepke, J. Reuder, M. Seefeldner, and D. Nowak, "Visualization of UV exposure of the human body based on data from a scanning UV-measuring system," Int. J. Biometeorol. **49**, 18–25 (2004).
44. J. E. Walsh, J. P. Bergmanson, D. Wallace, G. Saldana, H. Dempsey, H. McEvoy, and L. M. Collum, "Quantification of the ultraviolet radiation (UVR) field in the human eye in vivo using novel instrumentation and the potential benefits of UVR blocking hydrogel contact lens," Br. J. Ophthalmol. **85**, 1080–1085 (2001).
45. M. M. Sydenham, M. J. Collins, and L. W. Hirst, "Measurement of ultraviolet radiation at the surface of the eye," Invest. Ophthalmol. Vis. Sci. **38**, 1485–1492 (1997).
46. M. Coroneo, "Ultraviolet radiation and the anterior eye," Eye & Contact Lens **37**, 214–224 (2011).
47. M. Coroneo and S. Dain, "The sun and eyes: sunlight-induced eye disease and its prevention," *Sun, Skin and Health* (siro, 2014), p. 113.
48. M. S. Oliva and H. Taylor, "Ultraviolet radiation and the eye," International Ophthalmology Clinics **45**, 1–17 (2005).
49. J. E. Roberts, "Ultraviolet radiation as a risk factor for cataract and macular degeneration," Eye & Contact Lens **37**, 246–249 (2011).
50. A. R. Young, "Acute effects of UVR on human eyes and skin," Prog. Biophys. Mol. Biol. **92**, 80–85 (2006).

1. Introduction

Extended ocular UV exposure is well known to impact long-term ocular health (for review, see [1]). Whereas skin generally can efficiently be protected by textiles or application of sunscreens [2, 3], efficient everyday UV protection of the sensitive tissue of the eye and surrounding skin is a technological challenge. Sun glasses constitute the current standard protection of the eye against UV [4]. Australian sun glass standards are the common UV protection bench mark, those define light in the range of 315 up to 400 nm as harmful UVA [5, 6]. Although wearing of sun glasses is socially acceptable outdoors during sunny weather, its usage is not commonly accepted under all potential UV exposure conditions, such as during cloudy weather conditions as well as indoors [7]. Furthermore, practical reasons limit the use of (corrective) sun glasses to rather long-term UV exposure situations, as frequent exchange with corrective clear spectacles is cumbersome, furthermore storage of an extra pair of spectacles becomes necessary. But, harming UV exposure is not limited to extended outdoor stays in sunny weather. Instead, UV exposure constantly occurs, be it during short-term sun exposures while commuting to work e.g. within a car as a passenger while being exposed through the side windows [8–11], be it even indoors [12]. Thus, optimal UV protection will be reached if clear lenses efficiently minimize UV exposure as well.

In this work, clear lenses are compared according to their efficiency in ocular UV protection. Contributions to overall UV exposure are evaluated by simulating as well as measuring UV irradiances at the eye in a realistic geometrical simulation of the eye located within the human head, equipped with spectacle lenses. Experiment and simulation systematically assess the UV irradiance at the position of the eye by a sun-like light source. Irradiance is measured by a spectral sensor behind a diffusing plate. The following contributions to UV exposure are determined separately for all realistic angles of incidence of light: UV-light entering the eye through a clear spectacle lens (I_{direct}), UV light entering the eye bypassing spectacle lens and frame ($I_{indirect}$), as well as UV light entering the eye by back reflection from the lens surface (I_{back}), see Fig. 1. The impact of three spectacle lenses, designed to minimize ocular UV exposure is evaluated: a first spectacle lens, minimizing UV transmission through the lens (I_{direct}) up to 400 nm (L1 UV-block), a second spectacle lens, minimizing UV back reflections by an AR coating on the back side of the spectacle lens (L2 Back-UV), as well as a third spectacle lens combining both (L3 Combined).

The experimental results show, that the spectacle lens L1 UV-block, which minimizes the influence of I_{direct} reduces overall UV exposure down to 7 % relative to the naked eye. Only 1 % of the overall exposure at the naked eye originates from the back reflex, which is reduced to

Biomedical Optics EXPRESS

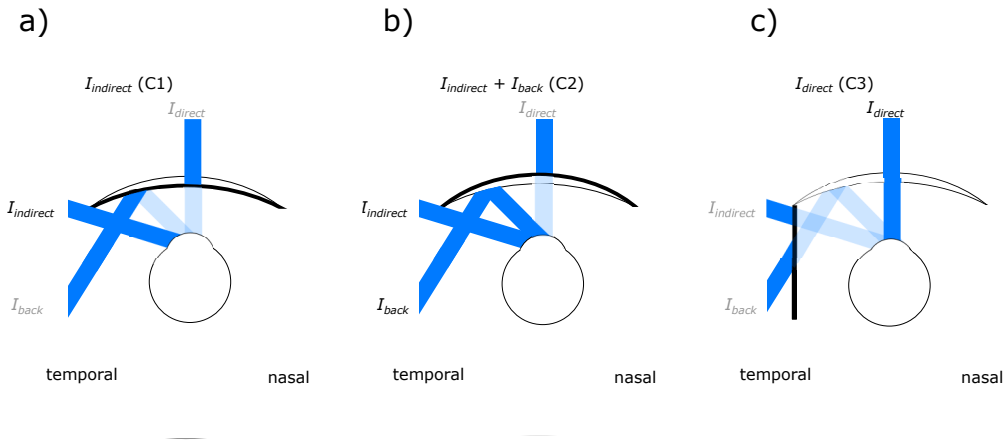

Fig. 1. Scheme of irradiance contributions, a) condition C1, contribution $I_{indirect}$, b) condition C2, contribution I_{back}, c) condition C3, contribution I_{direct}.

0.3 % by the spectacle lens L2 Back-UV. Spectacle lens L3 combines both benefits to reducing UV exposure to 6 %.

2. Methods

2.1. Study design

Clear lenses with single vision optical design, out of 1.5 organic material and with premium coatings were evaluated. A spectacle lens generally consists of three components, namely an organic lens substrate, a hard coating protecting the lens substrate, applied to both lens surfaces, as well as an anti reflection coating, determining the reflective properties of the lens surface. Figure 2 shows the schematic layout of the spectacle lens. UV protection is realized through either lens substrate or anti reflection coating. UV absorption of the lens substrate is increased through dedicated UV absorber. UV absorbers are a common additive in organic spectacle lens material, increasing material durability. But their absorbing properties do traditionally not reach up to 400 nm, as UV absorption in this range usually causes yellow tinting due to extension of absorptions into the blue VIS range. Therefore, the level of UVA protection to date was the result of a trade-off towards spectacle lens clarity. Thus, new products now focus on UV absorption specifically in the UVA range. Back-surface reflections are reduced by a specifically tailored anti reflection coating on the back surface.

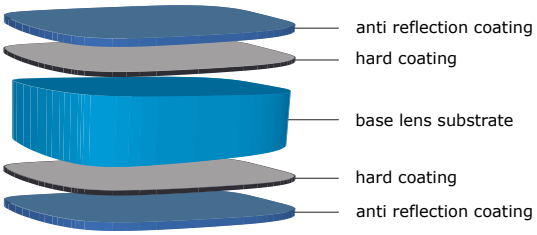

Fig. 2. Basic components of an organic spectacle lens: The main body of lens is plastic material (base lens substrate), protected by a hard coating of a few micron thickness and optionally equipped with an anti reflection coating on both sides. Layers are not in scale.

Biomedical Optics EXPRESS

Four spectacle lenses were evaluated, they varied in spectral absorption, mediated by the lens material, as well as in reflectivity of the back surface of the lens, mediated by the anti reflection coatings. UV transmission as well as reflection spectra of all used clear lenses are shown in Fig. 3. The first lens (lens L0, Basic) represents a standard clear spectacle lens, and is used as comparison to UV protective spectacle lenses. The second lens, L1 UV-block, shows increased UV absorption through optimized appliance of UV absorbers in the lens substrate. The third lens, L2 Back-UV, shows a decreased UV reflectance at the back surface of the lens, and thus intends to reduce UV back reflections. The fourth lens, L3 Combined, combines the UV absorbing substrate and the decreased UV reflectance at the lens back surface. All lenses had dioptric power zero ('plano lens').

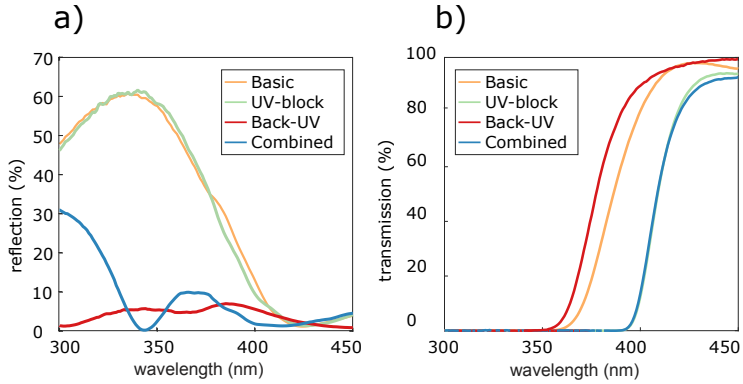

Fig. 3. a) Reflection spectra, as well as b) transmission spectra of the four clear lenses tested, measured at 6 deg with a spectrophotometer (type LAMBDA 950S UV/Vis Spectrophotometer by PerkinElmer Inc., Waltham, Massachusetts, USA).

2.2. Data simulation

A simulation was performed in MATLAB (MathWorks Inc., Natick, Massachusetts, USA). It contains a spherical spectacle lens of radius 87 mm with an oval shape of 56 mm width and 45 mm height, positioned at a back vertex distance of 17.5 mm, a wrap angle of 8 deg and a pantoscopic tilt angle of 5 deg. It furthermore contains a 3D avatar of the styropor mannequin head, recorded with a multicamera system (ZEISS VISUFIT 1000 by Carl Zeiss Vision International GmbH, Aalen, Germany). The male Caucasian mannequin head out of expanded polystyrene (type Styropor-Kopf männlich 30.5 cm by RAYHER, Laupheim, Germany) measured 21.0 cm from chin to top of the head, 16.5 cm from ear to ear, and 21.5 cm from tip of the nose to the back of the head with an interpupillary distance of 67 mm. The light source is simulated by a parallel grid of rays of the according azimuth and elevation angle with a ray distance of 0.3 mm. A plane detector with a diameter of 14 mm is placed at the surface at the position of the eyeball. Thus, irradiance was estimated at the ocular surface, and applies equally to the eye, eyelid, and eye-surrounding tissue. Clinical impact of the irradiance on the different ocular tissues is treated separately in the discussion.

Within the simulation the different irradiance contributions I_{direct}, $I_{indirect}$, as well as I_{back} are disentangled by the incidence angle and the number of refractions or reflections. Rays contribute to I_{direct} when coming from the frontal hemisphere, which equals azimuthal angles of 90 deg to -90 deg, and are refracted twice by the spectacle lens surfaces. Rays contribute to I_{back} when entering from the retral hemisphere, which equals azimuthal angles between -90 deg to -180 deg, and are reflected once at the back surface. Rays contribute to $I_{indirect}$ when hitting the sensor directly from the frontal hemisphere. I_{direct} is calculated as the sum of all rays with

Biomedical Optics EXPRESS

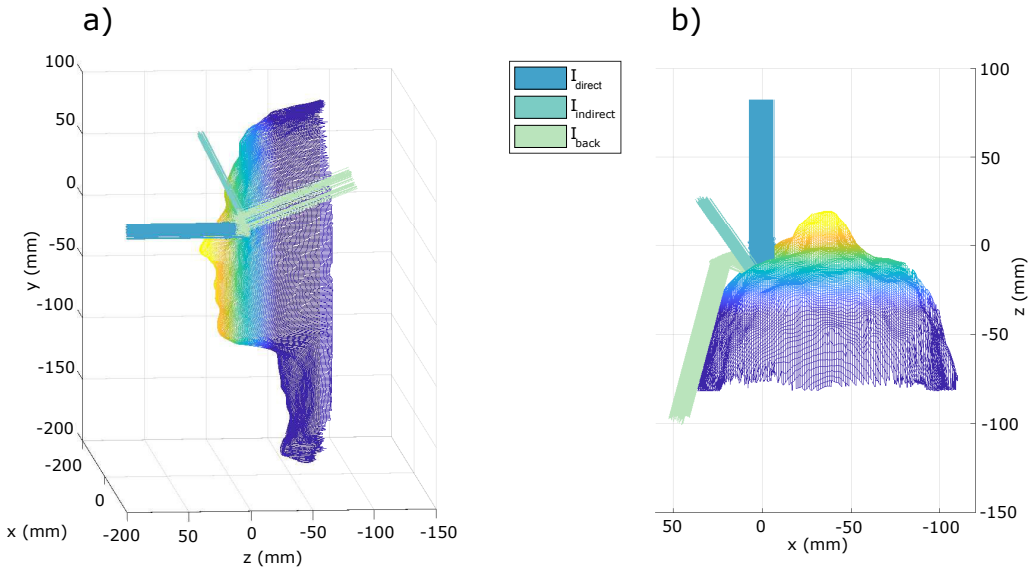

Fig. 4. Simulation of irradiance at the eye of a spectacle wearer: two views of avatar, spectacle lens, and a set of typical ray bundles of I_{direct}, $I_{indirect}$, and I_{back}.

an according transmission value T. I_{back} consists of the sum of all rays with their according reflexion coefficient $R(\lambda_i, \Omega)$, whereby the incident angle to the back surface of the lens Ω is taken into account. $I_{indirect}$ was calculated as sum of all rays without any weighting function. The transmission coefficient $T(\lambda)$ depends on the wavelength of the transmitted ray. It is weighted with the Xenon arc lamp spectrum. The reflection coefficient $R(\lambda_i, \Omega)$ was calculated forward from the design parameters of the coating as well as the reflection angle Ω and is weighted with the spectrum of the Xenon arc lamp in steps of 1 nm (type XBO 150W Xe OFR by OSRAM Licht AG, Munich, Germany).

The 3D avatar together with a set of typical rays is shown in Fig. 4. First evaluations show that the three contributions of irradiance originate from largely differing angles of incidence. Direct light I_{direct} enters the eye through the lens from a range of frontal angles. Indirect light $I_{indirect}$ bypasses the frame at oblique angles. In contrast, back reflected light I_{back} is found in the simulation for a rather restricted angular range from the back. Thus, a simulation of the full set of incidence angles at high angle sampling is executed. Furthermore, an experimental setup is designed to measure UV irradiances of a sun-like light source at the full range of angles of incidence selectively for the contributions of I_{direct}, $I_{indirect}$, and I_{back}.

Simulations as well as experimental measurements were performed for all four lenses.

2.3. Experimental procedure

Irradiance at the human eye was collected by a spectral sensor positioned behind a diffusing plate, placed at the position of the left eye in the mannequin head, positioned at the natural location of the cornea.

UV irradiance was measured by a UV VIS spectrometer (Insion UV VIS SENS /H Microspectrometer by INSION GmbH, Heilbronn, Germany) with CMOS linear image detector (type Hamamatsu S11639-01 by Hamamatsu Photonics K.K., Hamamatsu, Japan) through a Polytetrafluoroethylene (PTFE) diffusing plate, approximating a Lambertian radiator. Sensitivity of the spectrometer was larger than $16 * 10^{15}$ cts*nm/Ws at 450 nm and 650 nm. The PTFE

Biomedical Optics EXPRESS

diffusing plate had a diameter of 14 mm, an aperture of 12 mm, and a thickness of 2.2 mm. It was located at 23 mm distance from the end of the optical fiber that is connected to the spectrometer. Figure 5(a) shows the holder for the spectrometer fiber (dark red arrow) and the diffusing plate (light red arrow). The mannequin head was mounted on a rotatable platform, which allowed rotation of the head around the center of the diffusing plate along two axes, pitch and yaw, thereby simulating a change in elevation of the sun as well as different viewing directions of the head relative to the sun (Fig. 5(b)). A photo of the mannequin head is depicted in Figure 5(d). For simplicity, in the manuscript pitch of the mannequin head will be reported as elevation of the light source, thus allowing direct comparison to elevation angles of the sun. Mannequin head yaws will be reported as executed. UV irradiance was created by a Xenon arc lamp (type XBO 150W

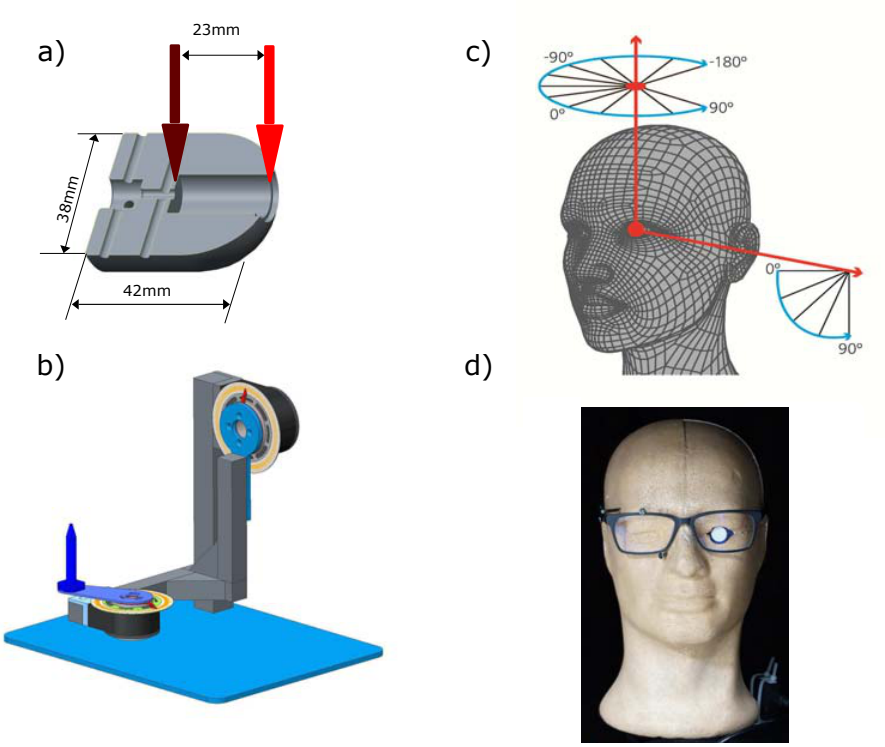

Fig. 5. a) Eye-shaped mount of spectrometer fibre and PTFE diffusing plate, arrows indicate position of the fiber (light red), and the diffusing plate (dark red), b) Mechanically rotatable mount of mannequin head, c) Schematic setup of head rotations, d) Photo of mannequin head, equipped with spectacle frame and sensor.

Xe OFR by OSRAM Licht AG, Munich, Germany), providing a broad UV spectrum. The UV spectrum of the light source is compared to D65 spectrum in Fig. 7(a). The source was positioned at a distance of 2.90 m from the spectral sensor, centered in front of the sensor center. A second spectrometer was used as permanent reference, illuminated by a fraction of the illuminating light reflected at a beam splitting silica glass plate. The beam splitting plate was placed at 45 deg in the illumination path. The reference spectrometer was equipped with an identical diffusing plate and holder. A schematic setup of the two light paths is shown in Fig. 6(b).

The mannequin head was covered with make-up (type essence camouflage 2in1 make-up & Concealer 30 honey beige by Cosnova GmbH, Sulzbach, Germany), which was tested to closely match the reflectance properties of skin. The spectrum of the make-up is shown in Fig. 7(b),

Biomedical Optics EXPRESS

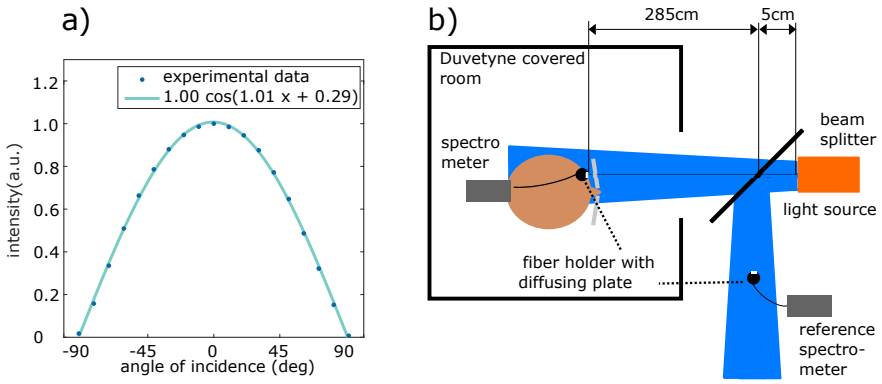

Fig. 6. a) Irradiance at sensor with varying azimuth, b) Schematic setup including head, light source and reference spectrometer.

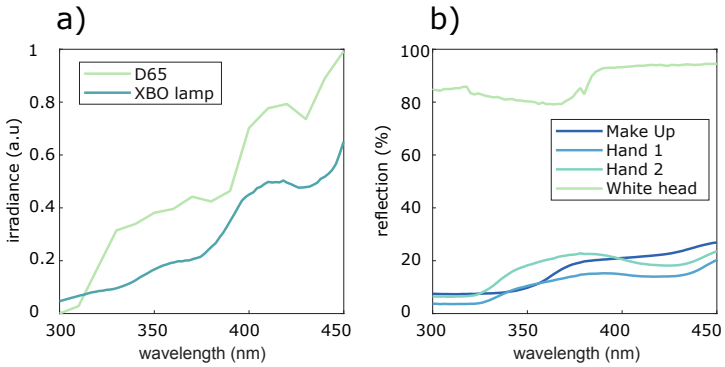

Fig. 7. a) D65 spectrum [13], compared to Xenon arc lamp spectrum, b) Reflection spectrum of make-up, white head, and two human skin samples.

together with spectra of two different hand skin samples and the spectrum of the naked styropor mannequin head out of expanded polystyrene without make-up.

The different clear lenses were inserted in the left lens position of a frame positioned on the mannequin head. All lenses were framed in the identical standard spectacle frame (type Menrad C39 Mod.11019-6699 56/16 140 MfL by Ferdinand Menrad GmbH+Co.KG, Schwaebisch-Gmuend, Germany). The frame was clipped tightly to the mannequin head behind a set of screws to ensure identical positioning of the frame and to prevent any minimal movement of the frame during rotation of the head. The right spectacle lens was a standard lens (type ZEISS Single Vision org. 1.5 DuraVision Platinum by Carl Zeiss Vision International GmbH, Aalen, Germany). Spectacle lenses L0, L1 and L3 had back radius of 87.5 mm, spectacle lens L2 had a back radius of 84.4 mm.

2.4. Spectral recording procedure

At the beginning of each measurement series, a dark current measurement was acquired. Figure 6(a) shows the irradiance decay at the sensor with increased azimuth, demonstrating the homogeneous illumination at the spectral sensor.

Spatial inhomogeneity of the light source was controlled. In the case of back reflections a correction factor of 1.13 was introduced counteracting a decay of intensity of the back reflected light. It was based on repeated radiometric measurements of the incident light intensity back

Biomedical Optics EXPRESS

reflected to the eye relative to the light incident from straight ahead. Based on Fresnel equations the degree of polarization of the incident light is expected to be < 5 %.

Each spectrum was acquired as average of 10 measurements. Spectra were automatically calculated relative to dark current of the respective measurement series. Reference signal variance was 1.6 % over the whole measurement series with a maximum of 3.6 %, providing an irradiance stability of 96.4 %.

In each condition, the UV spectrum from 350 nm to 400 nm was analyzed. Head yaws from 90 deg (light coming from the right side towards the nose) to -180 deg (light coming from the back) were sampled at 4.5 deg, and solar elevations equivalents from 0 deg to 90 deg in steps of 22.5 deg, thus assessing the full range of potential irradiance orientations. Figure 5(c) summarizes the set of recording orientations. Integrated and peak irradiances are reported for all clear lenses.

Table 1. **List of measurement conditions**

Cond	B	$C1$	$C2$	$C3$
I_x	I_{all}	$I_{indirect}$	I_{back} $+I_{indirect}$	I_{direct}
realization	no cover	back covered	front covered	blinders
without frame	x	-	-	-
empty frame	x	x	-	x
Basic L0	x	-	x	x
UV-block L1	x	-	x	x
Back-UV L2	x	-	x	x
Combined L3	x	-	x	x

A set of four measurement conditions was defined to disentangle the contributions of I_{direct}, $I_{indirect}$ and I_{back}, see Fig. 1 and Table 1. The conditions varied in covering or shading of lenses or diffuse irradiance assessment area. In addition, one baseline is recorded, measuring overall irradiance I_{all} without any modification (B). It is recorded without frame, with an empty frame as well as all four lenses. The contribution of $I_{indirect}$ is evaluated by a condition, in which the backside of the spectacle lens is covered (C1). As there is no contribution of the clear spectacle lens, it is measured only once. The contribution of I_{back} is determined by a condition with the frontside of the spectacle lens covered (C2). It is measured for all four spectacle lenses. The contribution of I_{direct} is evaluated by a condition, in which $I_{indirect}$ and I_{back} are blocked by blinders (C3). Condition C3 is evaluated for all four lenses as well as the empty frame. The different light source orientations are recorded in one block, for each condition separately. Overall 16 conditions were recorded.

2.5. Data analysis

Data preparation included the following four steps: clipping, integration, solid angle correction, and normalization to overall irradiance without frame. In the first step, I_{direct} data were clipped to zero at 340 nm ± 15 nm for each solid angle separately. This is valid, as in this wavelength range, UV transmission measured in I_{direct} is zero in all tested clear lenses (see Fig. 3). Identical clipping factors are applied to I_{all}, which is largely dominated by I_{direct}. Thereafter, data from 350 nm to 400 nm was integrated. Acquired counts per solid angle are weighted according to the surface area the grid patch of the solid angle spans on a reference sphere. Finally, all irradiances are normalized to the integrated irradiance of the naked eye. All irradiances will thus be reported in percentage of overall irradiance at the naked eye. As condition C2 contained indirect light together with light back-reflected from the spectacle lens surface, all following calculations of I_{back} are restricted to the area of the well-defined small area of the back reflex, namely an

Biomedical Optics EXPRESS

azimuthal range of 157 deg to 175 deg, and an elevation of 22.5 deg.

In a first step, average I_{direct} (C3), $I_{indirect}$ (C1), as well as I_{back} (C2) are calculated for all four tested clear lenses (L0 Basic, L1 UV-block, L2 Back-UV, L3 Combined), integrated over all elevations and yaws. Errors are estimated as standard deviations together with condition B, which contains the sum of all three irradiance contributions. For condition C2, B of the according angular area was taken as reference, $I_{all} - I_{direct}$ served as reference for $I_{indirect}$, and $I_{all} - I_{indirect}$ for I_{direct} respectively. In a second step, relative irradiances are analyzed spatially. Peak irradiances are reported. Furthermore, integrated irradiances at different solar elevations are analyzed, and different head yaws relative to the sun. Finally, 2D spherical maps of irradiances detail relevant incidence angles of the three irradiance contributions I_{direct}, $I_{indirect}$, and I_{back}.

3. Results

Figure 8 shows a clear picture of ocular irradiances with the tested clear lenses relative to the naked eye. Already 18 % of the incoming irradiance is filtered by a frame. Of the remaining irradiance, the vast majority (79 ±3 % of the overall irradiance at the naked eye) is entering the eye through the empty spectacle frame. When equipping the frame with the clear spectacle lens L0 Basic, the contributions of I_{direct} constitutes 32 ±4 % of the overall irradiance at the naked eye, whereas overall irradiance is 83 ±5 % of the overall irradiance at the naked eye. Thus, although reduced, still the majority of UV enters the eye through the spectacles. In our example, only 3.1 ±2.6 % of the overall irradiance at the naked eye is coming from indirect light bypassing the frame.

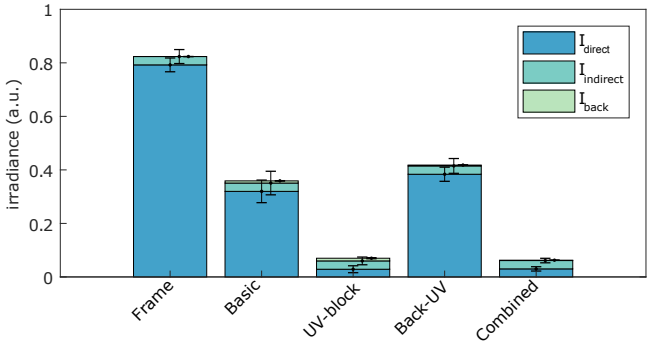

Fig. 8. Overview on experimental data of UV irradiances reaching the eye integrated in the range of 350 - 400 nm. I_{direct}, $I_{indirect}$, I_{back} as stacked bar charts for empty frame as well as four different clear lenses.

Figure 9 compares irradiance contributions between the analyzed clear lenses, L1 UV-block, L2 Back-UV, as well as L3 Combined in experiment and simulation. When comparing the three spectacle lenses to the Basic lens L0, the most dominant protective effect occurs for I_{direct}. It is clearly visible, that I_{direct} is strongly diminished by the spectacle lens UV-block. The overall irradiance is reduced to only 7 ± 3%.

When comparing simulated and experimental data in Fig. 9, the simulated data show a slightly smaller I_{direct} in the lenses L1 UV-block, as well as L3 Combined. When looking specifically at the contribution I_{back}, lenses L2 Back-UV and L3 Combined are significantly decreased in both simulation and experimental data (Fig. 9(b), 9(d)). Experimentally the irradiance reduction of I_{back} by lens L3 Combined seems to be slightly overestimated, whereas the reduction of I_{back} by lens L2 Back-UV is underestimated in comparison to the simulation.

Biomedical Optics EXPRESS

When simulating the contribution of the higher energy irradiance in the range of 300 - 350 nm, covering the relevant range within the UV of D65, the contribution of I_{back} increases to up to 4 %, whereas the impact of I_{direct} vanishes. Therefore, the measured range of 350 - 400 nm constitutes the relevant wavelength window of UVA with respect to ocular protection.

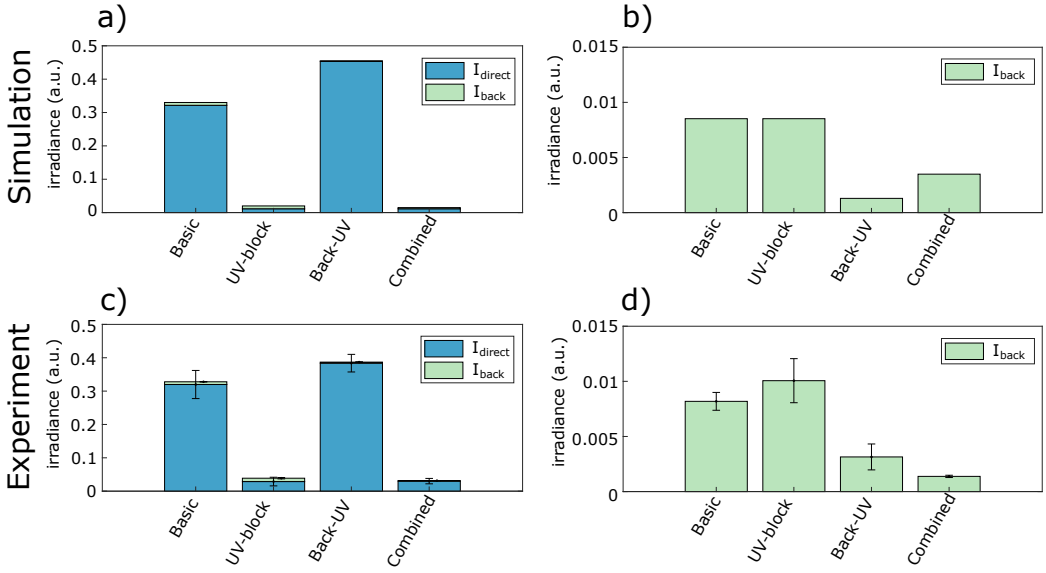

Fig. 9. Simulation (a) and experimental data (c) of UV irradiances reaching the eye integrated in the range of 350 - 400 nm. I_{direct}, and I_{back} as stacked bar charts the for four different clear lenses. b) Simulated integrated irradiance contributions of back-reflected irradiances for the four different clear lenses, together with d) experimental data for comparison.

Depending on the incidence angle of the light, irradiance contributions of direct and back-reflected light vary. Thus, in a second step, peak irradiances are evaluated, determining the worst case scenario. In Fig. 10(b), peak I_{direct}, as well as I_{back} of all four clear lenses are reported together with the simulated contributions in Fig. 10(a). Please note, that the overall level of the peak irradiances depends on angular sampling of the dataset. Frontal illumination is contributing strongest to I_{direct} (head yaw 5.6±8.5 deg/sun elevation 0±0 deg).

I_{back} peaks when illuminating from the back (head yaw -165.5±2 deg/sun elevation 22.5±0 deg) in the experiment I_{back} peak irradiances are relatively high in comparison to the integrated contribution of I_{back}. This hints towards a reflection pattern confined in angular space. Nonetheless, it is still smaller than I_{direct} in lens L0 Basic.

When comparing irradiances at different sun elevations in Fig. 11, it is nicely visible that I_{direct} and I_{back} are strong for small sun elevation angles. The simulation in Fig. 11(a)-(d) specifically demonstrates the broad distribution of I_{direct} as well as the rather confined occurrence of I_{back}. It is furthermore nicely visible, that the reduction of I_{direct} by lens L1 UV-block fully applies to the broad range of elevations, in which a significant amount of I_{direct} occurs. In contrast, reduction of I_{back} by lens L2 Back-UV is restricted to the very narrow range of elevation, in which a significant contribution of I_{back} occurs. Irradiances for different head yaws are shown in Fig. 12. The quasi symmetric shape of I_{direct} around the central position is clearly visible, as well as the directionally strongly limited occurrence of I_{back}. Only at -166.5 deg, a sharp, but noticeable amount of I_{back} occurs with a width of less than 20 deg. In Fig. 12(a)-(d) the simulated average irradiance is shown depending on head yaw angle relative to the light source. Not only peak

Biomedical Optics EXPRESS

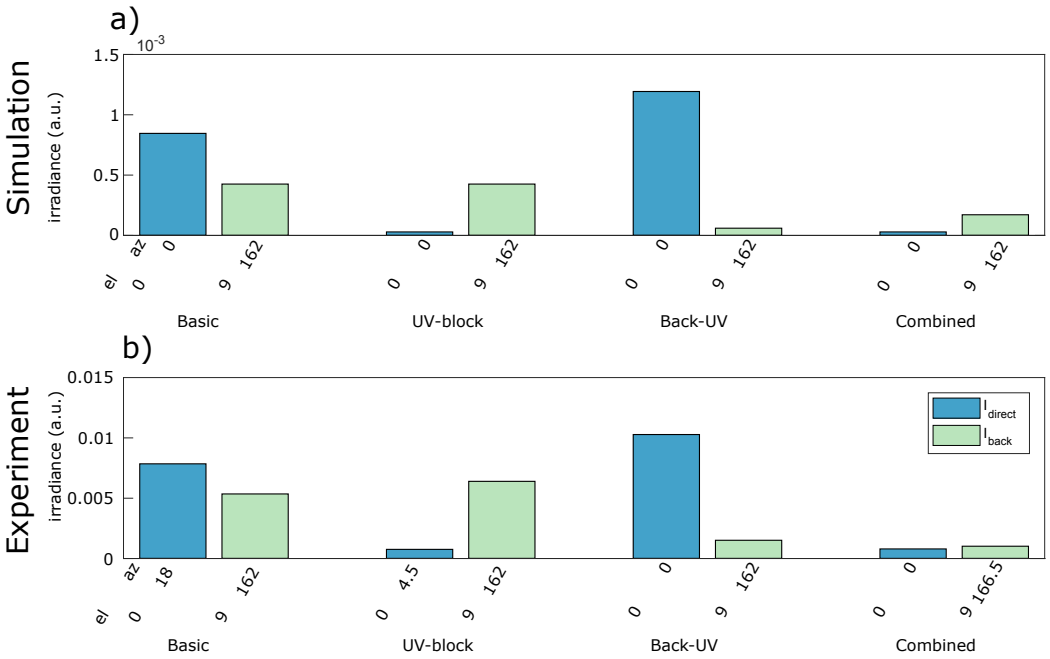

Fig. 10. Maximal UV irradiances reaching the eye. (a) Simulated peak irradiances, as well as (b) Experimentally measured peak irradiances, together with angles of occurrences (elevation/head yaw) in I_{direct}, and I_{back} for the four different clear lenses.

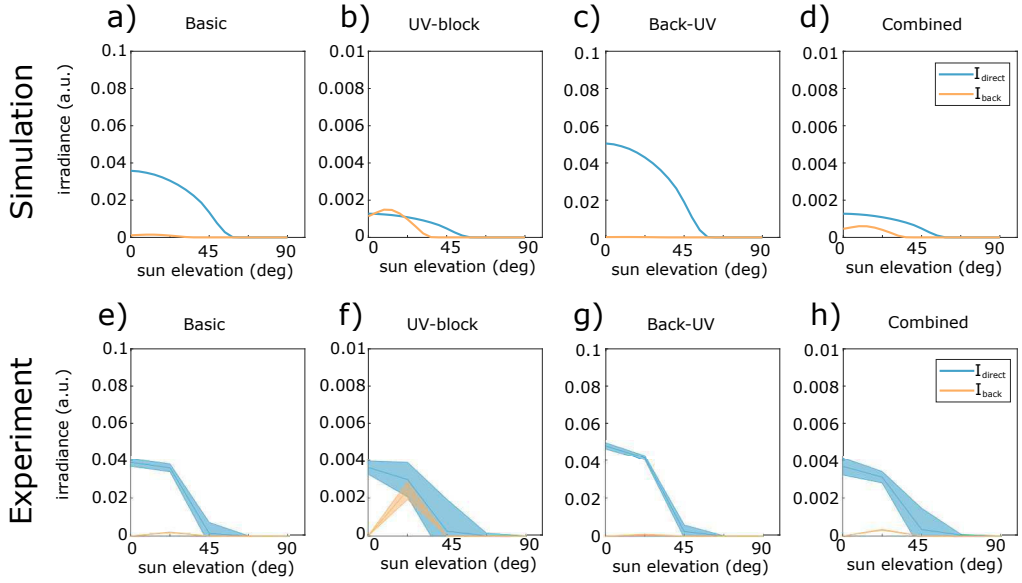

Fig. 11. Simulated (a-d) and experimentally measured (e-h) UV irradiances reaching the eye. I_{direct} (blue), and I_{back} (red) for a, e) L0 Basic, b, f) L1 UV-block, c, g) L2 Back-UV, as well as d, h) L3 Combined as function of elevation angle, shaded error bars represent standard deviations from I_{all}.

Biomedical Optics EXPRESS

position and shape of I_{back} match nicely, even a slight shift of I_{direct} from the nasal direction at positive azimuthal angles is replicated by the model, originating in the asymmetric placement of the spectacle lens in front of the eye next to the nose. In both, sun elevations as well as head yaws, angular distributions of irradiances resemble each other among the different clear lenses. Between them, mainly the overall level of the different irradiance contributions varies.

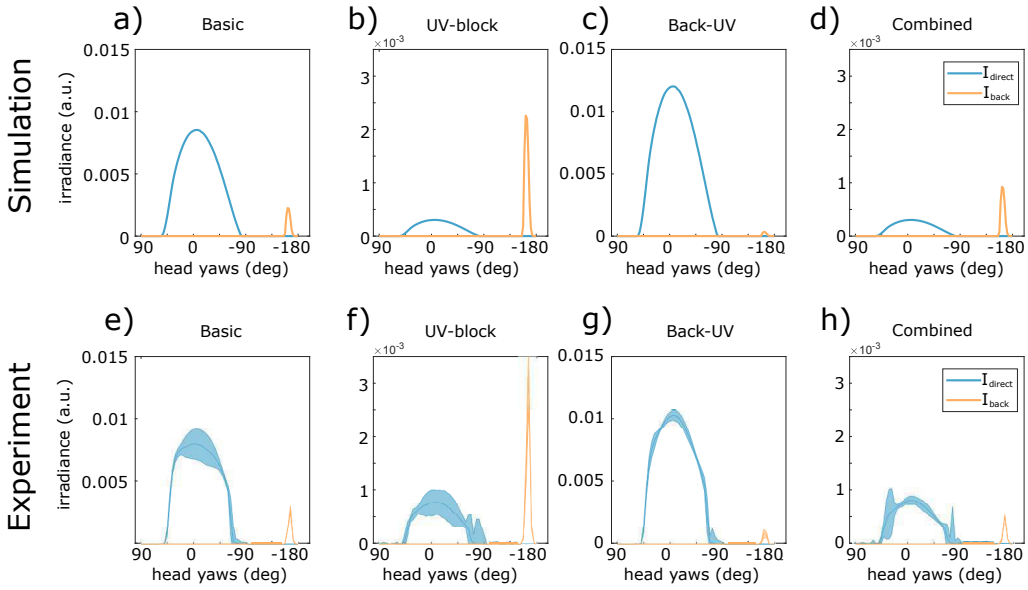

Fig. 12. Simulated (a-d) and experimentally measured (e-h) UV irradiances reaching the eye. I_{direct} (blue), and I_{back} (red) for a, e) L0 Basic, b, f) L1 UV-block, c, g) L2 Back-UV, as well as d, h) L3 Combined as function of head yaws, shaded error bars represent standard deviations from I_{all}.

When mapping the measured irradiances of the contributions I_{direct}, $I_{indirect}$ and I_{back} on a sphere, the characteristic angular distributions are well visible. Figure 13 shows such a map exemplary for lens L0 Basic. I_{direct} is distributed broadly over illuminations from the front, with a stronger spread in azimuth, than in elevation. $I_{indirect}$ is showing contributions from both sides, showing an almost ring-like structure. In the simulation, the ring-like structure is more dominant. Deviations originate from the fact, that simulation lacks occlusions due to a spectacle frame. Therefore, the contribution of $I_{indirect}$ is much larger in the simulation as well, stressing the impact of frame shape, size and fit on the indirect light. I_{back} is forming a sharp peak from the posterior hemisphere. Please note that for better visibility the contribution of I_{back} is inverted on the y-axis, changing from 'front-back' to 'back-front'.

4. Discussion

The main contribution to ocular UV exposure originated from direct exposure (I_{direct}), be it with an empty frame (79 %) or clear spectacle lens L0 Basic (31 %). Contributions of indirect irradiance ($I_{indirect}$) constituted only 3 % of the overall irradiance of the naked eye. Lens L0 Basic thus reduces direct exposure down to approximately a third of the irradiance of the naked eye, but adds a small irradiance of approximately 1 % through back reflections (I_{back}), more than an order of magnitude smaller than I_{direct}. An overall reduction of exposure to 7 % was achieved by spectacle lens L1 UV-block, whereas lens L2 Back-UV reduced exposure to 42 %. Spectacle lens L3 Combined reduced irradiance to 6 %. Although I_{back} reached comparable peak values as

Biomedical Optics EXPRESS

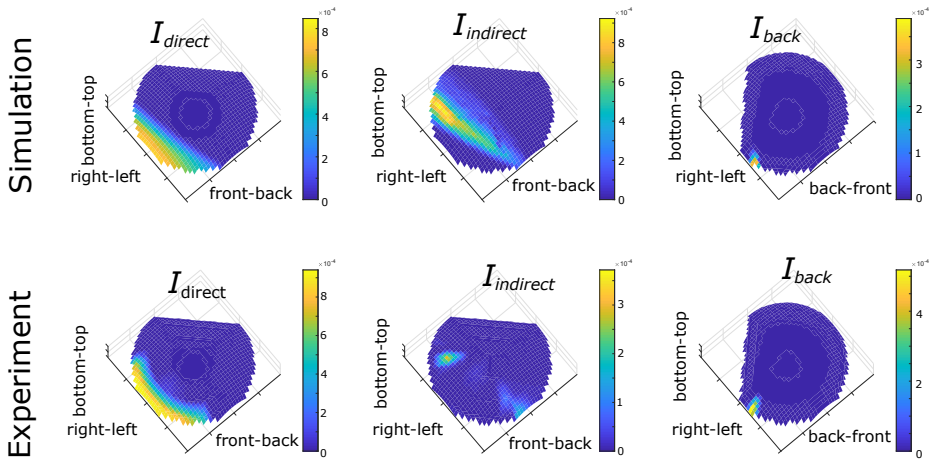

Fig. 13. Surface maps of experimantally measured as well as simulated irradiance contributions I_{direct}, $I_{indirect}$, and I_{back} of lens L0. Right/left indicates that the light is coming from the right/left side, front/back indicates that the light is coming from the front/back and bottom/top indicate that the light is coming from the horizon/zenith. Colorcodes show magnitude of irradiance in units of the overall irradiance at the naked head. For visualization purposes irradiances are interpolated to a grid of 0.025 unit radii.

I_{direct} in lens L0 Basic, the overall reflection was very confined in angular space, and thus would seldomly be matched in natural behavior. I_{direct} was much broader in angular space, leading to a more powerful reduction of irradiance by clear lenses L1 UV-block and L3 Combined.

Simulations confirmed the overall contributions of the different types of irradiances, replicating magnitudes and angular distributions in a higher angular resolution. One specific difference between simulation and experiment constituted the shading effects of the frame reducing the indirect light in the experiment.

Experimental limitations were mainly imposed by the repeatability of the exact position of the frame on the mannequin head. Impact of the frame position was minimized by a fixation of the frame with screws on the mannequin head. Smaller contributions to experimental variations were introduced by the repeatability of the spectrometer measurements, and slight variations in light source intensity, as well as spatial illumination profile. Both were carefully characterized. Differences in I_{back} in lens L2 Back-UV compared to the others might have been introduced by a deviating lens curvature.

The experimental conditions I_{direct}, $I_{indirect}$, and I_{back} included some simplifications, which were considered small. Although $I_{indirect}$ does not include back reflections from the spectacle lens, which was covered, it does include back reflections of the frame. I_{back} neglects contributions of multiple reflections of light entering from the front.

From the literature, it is known that clear lenses contribute to ocular UV protection [14, 15]. But, awareness of the approach is limited in comparison to ocular UV protection through sun glasses. Information on the efficiency of UV protection by clear spectacle lens was perceived as rather confusing and unclear to practitioners and consumers [16]. In fact, the efficiency of UV protection (through limited UV transmission, equivalent to UV-block) has been shown to effectively prevent UV related ocular damage in mice recently [17]. Recent publications brought a potential danger of back reflections from spectacle lens back surfaces into play [18, 19]. The presented data now clarifies two aspects of UV protective effects of clear spectacle lenses. First,

Biomedical Optics EXPRESS

high protection levels are reached in clear spectacle lens L1 UV-block, reducing UV exposure by more than an order of magnitude. Secondly, back reflections contribute only insignificantly to overall ocular UV exposure.

It is furthermore known, that contributions to ocular UV exposure from indirect as well as back-reflected light can additionally be minimized by a beneficial choice of spectacle frame as well as a carefully adjusted position of wear [14, 20, 21]. Larger frames with broader temples efficiently shadow UV. Careful fitting of frames prevents leakage of UV from the side. Specifically the comparison between simulation, which does not include a spectacle frame, and experimental data, which includes a spectacle frame, in Figure 13 shows the impact of a well-fitted frame on $I_{indirect}$, namely UV light entering the eye from the side. The present dataset demonstrates ocular UV irradiances in a controlled laboratory surrounding, individual all-day UV doses vary distinctly based on environmental and behavioral factors. Significant differences in UV exposure have been shown depending on textural and topographic properties of the environment, varying reflectivity even differently throughout the day. Beach environments have been shown to provide stronger UV levels than grass surroundings [22], valley like arrangements of the surrounding topography have shown highest exposure levels under full illumination [23]. Reflectivity of the surrounding textures has been shown to significantly impact ocular UV doses as well [12, 24–26]. Additionally, increased altitude as well as ozone levels are well-known to increase UV doses [12, 27, 28]. During the day, ocular UV exposure varies. Strongest exposure from direct sun light is expected under sun elevation angles between 30 deg and 50 deg [29–35]. These results are well in line with the low elevation angles found for direct, indirect, as well as back-reflected light. The time during the day, in which these angles are reached, varies with latitude. Generally ocular UV exposure shows a bimodal distribution with peak exposure times during morning and evening. Thus, specifically in the morning and evening times, in which the solar elevation is low, spectacle lens wearers benefit from UV protecting lenses. The impact of diffuse light is less time dependent, and most relevant from the top [36, 37]. In sum, overall ocular UV exposure is a conglomerate of direct, indirect exposure and exposure reflected from the surrounding, varying differently diurnally [39]. UV doses during cloudy weather conditions have been shown to significantly contribute to overall UV doses, thus stressing the importance of all-day ocular UV protection [38].

Additionally, individual behaviors and habits strongly shape ocular UV doses. Girls have been shown to expose themselves stronger to UV compared to boys [11], outdoor workers have been shown to collect greater UV doses compared to indoor workers and adolescents [12]. Maximum exposure in terms of sun elevation angles clearly depends on head posture, which has been shown to vary, even depending on the task [11, 34, 40]. In a direct comparison of different body postures, forehead UV exposure was strongest for sitting and lying postures [25]. In these situations, in which the head is tilted towards the sun, spectacle lenses provide specifically efficient protective effects. Due to the plurality of factors influencing individual UV exposure, strong efforts have been made to estimate UV-exposure from UV dose readings at different inclinations as well as inclination estimations of human body surface [41–44]. Estimates of ocular UV exposure from general UV exposure range from 2 % – 23 % [24, 45], indicating a significant impact on the sensitive ocular tissue and surrounding skin. The detrimental impact of UV on ocular health has been described in detail in numerous reviews, stressing the relevance of ocular UV protection [1, 46–50]. Eyelid, ocular surface, as well as crystalline lens have been shown to be impacted by UV irradiance [1]. Clinical relevance of ocular UV exposure varies with incidence angle. Whereas eyelid, and ocular surface are affected strongest by direct irradiance, peripheral UV exposure has been related to pterygium, pinguecula and cortical spoke cataract [46]. Direct exposure is minimized with an appropriate choice of spectacle lens, such es lens L1 or L3 of the present study. A careful selection of frame best minimizes peripheral exposure through indirect UV.

Thus, instead of limiting ocular UV protection to situations subjectively judged as critical,

Biomedical Optics EXPRESS

all-day wear of clear lenses optimized for UV irradiance reduction optimally protects eye and surrounding tissue from UV.

5. Conclusion

Three spectacle lenses minimizing UV irradiance at the eye (UV-block, Back-UV, and Combined) were simulated and subsequently evaluated experimentally with respect to sun irradiance at the eye. UV irradiance was evaluated by a spectral sensor, which was placed behind a diffusing plate. By more than an order of magnitude more irradiance reached the eye through the spectacle lens, compared to light, back-reflected from the lens surface. Thus, clear lenses with a tailored UV absorber efficiently protect the eye from UV, supplementing sun glasses wear to an all-day protection scenario.

Acknowledgments

The authors thank Norbert Kurz, Martin Amberg, Robert Faul, Alexander Keckeisen, Dmytro Dubson, Josef Fixel, and Thomas Schirle for technical support, Artur Laukart for calculation of reflection coefficients, Patrick Schaupp and Christian Lappe for design support of the illustrations.

Disclosures

CG: Carl Zeiss AG, KR: Carl Zeiss Vision International GmbH (E), MH: Carl Zeiss Vision GmbH (E), RB: Carl Zeiss Vision GmbH (E), RS: Carl Zeiss Vision GmbH (E), SW: Carl Zeiss Vision International GmbH (E), TM: Carl Zeiss Vision International GmbH (E)